Abnormal behavior of the optical potential for the halo nuclear system ^{6}He + ^{209}Bi

L. Yang (杨磊),[1,2] C. J. Lin (林承键),[1,3,*] H. M. Jia (贾会明),[1] D. X. Wang (王东玺),[1] N. R. Ma (马南茹),[1] L. J. Sun (孙立杰),[1] F. Yang (杨峰),[1] X. X. Xu (徐新星),[1,4] Z. D. Wu (吴振东),[1] H. Q. Zhang (张焕乔),[1] and Z. H. Liu (刘祖华)[1,†]

[1]*China Institute of Atomic Energy, P.O. Box 275(10), Beijing 102413, China*

[2]*Center for Nuclear Study (CNS), University of Tokyo, RIKEN Campus, 2-1 Hirosawa, Wako, Saitama 351-0198, Japan*

[3]*College of Physics and Technology, Guangxi Normal University, Guilin 541004, China*

[4]*Department of Physics, The University of Hong Kong, Pokfulam Road, Hong Kong SAR, China*

(Received 7 August 2017; published 18 October 2017)

In a recent transfer reaction measurement of ^{208}Pb(^{7}Li,^{6}He)^{209}Bi at energies around and below the Coulomb barrier, the optical model potentials of the halo nuclear system ^{6}He + ^{209}Bi were extracted by fitting the experimental data with the theoretical frameworks of the distorted-wave Born approximation and coupled reaction channels, respectively. With the high-precision result, a complete picture of the behavior of the optical potential for this halo system is clearly derived for the first time. The real potential presents a bell-like shape around the barrier as a normal threshold anomaly. However, for the imaginary part, it first increases with the energy decreasing below the barrier and then falls quickly to 0, hence the threshold energy can be determined by fitting the variation trend. Moreover, the result also provides some evidence that the dispersion relation does not hold for this halo nuclear system, which calls for further investigation of the underlying physics.

DOI: 10.1103/PhysRevC.96.044615

I. INTRODUCTION

The phenomenological optical model potential (OMP) is usually adopted to describe the complicated interaction of two nuclei, which can be expressed as a complex mean-field effective potential [1], i.e., the real part of the potential is used to describe elastic scattering, while nonelastic processes which lead to the loss of flux from the elastic channel can be represented by the imaginary term. With decades of research, the basic properties of OMPs of tightly bound systems have been recognized, e.g., when the interaction energy gets close to the Coulomb barrier, a strong energy dependence is present in both the real and the imaginary parts due to strong couplings between intrinsic and relative motion degrees of freedom, which is known as the threshold anomaly [2,3]. This behavior is characterized by a sharp decrease in the imaginary part as the bombarding energy decreases towards the Coulomb barrier, associated with a localized bell-shaped structure around the barrier in the real part. The dispersion relation, which is based on the causality principle, can be used to connect the real and imaginary parts [3,4]. Nowadays, the OMPs of weakly bound systems have attracted great interest [5–7], because of the particular properties of the potential arising from the exotic nuclear structure. The extended valence nucleon distribution will favor the processes of breakup and transfer, and the dynamical effects will be further reflected by the OMP. For example, in order to reproduce the angular distribution of elastic scattering of the halo nucleus ^{6}He, in addition to the effect of Coulomb dipole polarizability [8–11], a large diffuseness parameter of the imaginary part is required to respond to the long-range absorption [11–13]. Moreover, even when the energy is lowered below the Coulomb barrier, the depth of the imaginary potential increases as the energy decreases, indicating that the absorption continues to be strong. This abnormal behavior is naturally associated with the breakup reaction, due to the low separation energy of weakly bound nuclei. Thus this phenomenon is the so-called breakup threshold anomaly [14–17]. However, the fundamental reason is still unclear.

So far, most research has employed stable weakly bound projectiles, such as ^{6,7}Li and ^{9}Be [5]. Due to experimental difficulties, only a few investigations have been performed on the radioactive halo nuclei, like ^{6}He [11,14,18], ^{7}Be, and ^{8}B [19]. However, because of the large data uncertainties as well as the lack of enough data points [11,16], it is nearly impossible to investigate the optical potentials of halo systems in the subbarrier region directly with low-intensity radioactive ion beams. Even for stable weakly bound systems, we are still far from a clear understanding of the properties of OMPs, e.g., the behavior of the potential in the deep subbarrier region leaves much to be desired [5,20,21], and the application of the dispersion relation is still debatable [4,17,18,22].

In view of this fact, a transfer reaction method [23] was proposed to study OMPs of halo systems by the utilization of a stable beam, which can yield fairly precise results. The sensitivity of this method has been examined [24], which provides a solid theoretical reference for the application of the transfer method. And experimental attempts have been made to study OMPs of the weakly bound nuclear systems ^{17}F + ^{13}C [25] and ^{6}He + ^{12}C [26]. Recently, we have further applied this method to study optical potentials of the halo systems ^{6}He + ^{209}Bi [18] and ^{64}Zn [27], with the one-proton transfer reactions ^{208}Pb(^{7}Li,^{6}He) and ^{63}Cu(^{7}Li,^{6}He) induced by the stable beam ^{7}Li at energies around and above the Coulomb barrier, respectively.

In the previous work [18], an increasing trend toward an imaginary potential with energy decreasing in the subbarrier

*Corresponding author: cjlin@ciae.ac.cn
†Deceased.

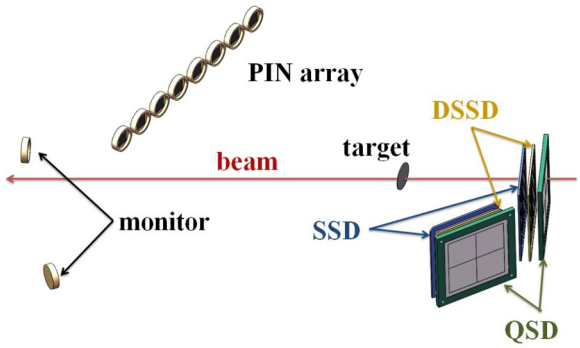

FIG. 1. Schematic of the experimental setup.

region was observed clearly in the halo system ^{6}He + ^{209}Bi for the first time. However, the energy was too high to explore the threshold region, which contains critical information to examine the applicability of the dispersion relation. To investigate further the potential of ^{6}He + ^{209}Bi in the deep subbarrier region, a new experiment was performed at sufficiently low ^{7}Li incident energies.

Following the previous paper [28], we give here the details of this work. The paper is organized as follows. Section II describes the experimental procedure and results. Section III presents the calculation results using different theoretical frameworks, as well as discussing the energy dependence of the extracted OMPs. A summary and conclusions are given in Sec. IV.

II. EXPERIMENTAL PROCEDURE

The experiment was carried out at the China Institute of Atomic Energy, Beijing, with the ^{7}Li beam accelerated by the HI-13 tandem accelerator to the energies of 21.20, 24.30, 25.67, and 28.55 MeV. The isotopically enriched ^{208}Pb (99.7%) target, with a thickness of about 120 μg/cm^2 on a 20 μg/cm^2 carbon backing, was bombarded by the ^{7}Li beam, with a current of about 40 pnA. The angle between the target and the beam direction is about 72°. A schematic of the experimental setup is given in Fig. 1. Two silicon-PIN-diode detectors were placed at ±15° relative to the beam direction to monitor the beam quality and normalize the experimental data, since pure Rutherford scattering is expected at such forward angles. An array including eight PIN detectors covering the angle from 20° to 68° was mounted to measure the elastic scattering of the entrance channel ^{7}Li + ^{208}Pb. The typical energy spectrum from a single PIN detector is shown in Fig. 2, where one can see that the inelastic scattering peak of the first excited state of ^{7}Li ($E^* = 0.48$ MeV) can be distinguished from the elastic scattering one. The obtained elastic scattering angular distributions of ^{7}Li + ^{208}Pb are shown in Fig. 3, where only the statistical error is considered.

Two additional Si-detector telescopes were fixed in the backward angle region to measure the transfer reaction product ^{6}He. Each telescope consists of three layers of Si detectors: the first layer is a 20-μm single-side strip detector (SSD, 16 channels), followed by a 60-μm double-sided strip detector (DSSD, 16 × 16 pixels) and a 1-mm-quadrant silicon detector

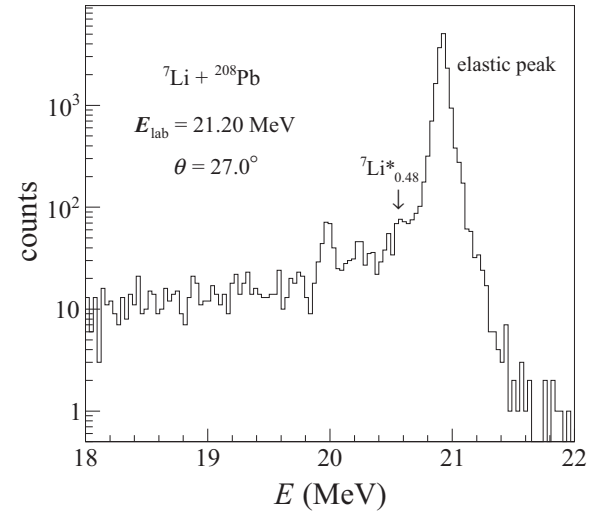

FIG. 2. Typical energy spectrum obtained by a single PIN detector at $E_{lab}(^{7}\text{Li}) = 21.20$ MeV and $\theta_{lab} = 27.0°$.

(QSD) as the residual energy (E_R) detector. The active area of each telescope is 50 × 50 mm^2, with angular coverages of 99°–127° and 144°–171°, respectively. The ΔE-E_R spectrum obtained by the telescopes at the highest energy, E_{lab} = 28.55 MeV, was illustrated in Ref. [28]. It can be seen that the transfer products ^{6}He can be identified clearly from the scattered ^{7}Li as well as the helium isotope ^{4}He. Moreover, the resolution of the telescope is high enough to identify different transfer reaction final states, which corresponds to one proton transferred to different single-particle states of ^{209}Bi. However,

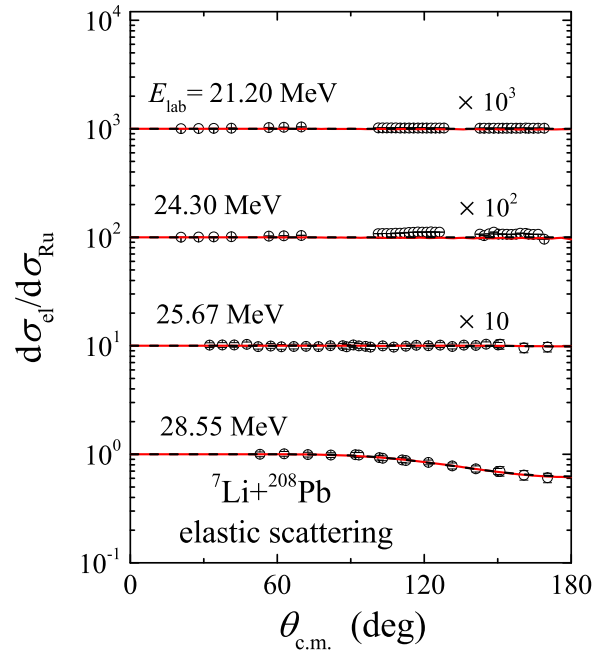

FIG. 3. Angular distributions of elastic scattering of the ^{7}Li + ^{208}Pb system. Open circles represent experimental data. Solid and dashed curves show fitting results from the CRC and OM calculations, respectively.

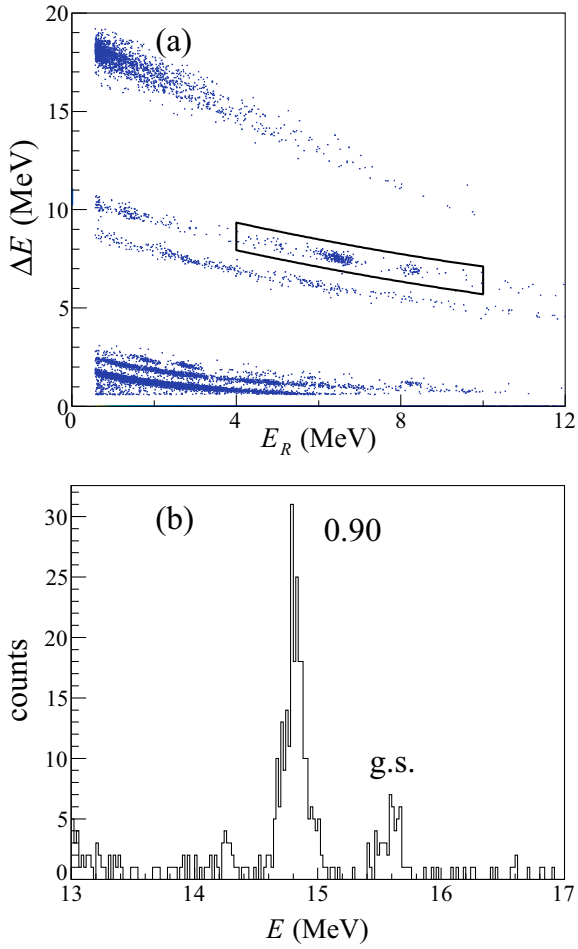

FIG. 4. (a) ΔE-E_R spectrum obtained by the telescope at $E_{\rm lab}$ = 24.30 MeV with $\theta_{\rm lab}$ = 144°–171° and (b) projected energy spectrum of the selected ^{6}He band, where the peaks are labeled corresponding to the excitation energies of ^{209}Bi (in MeV).

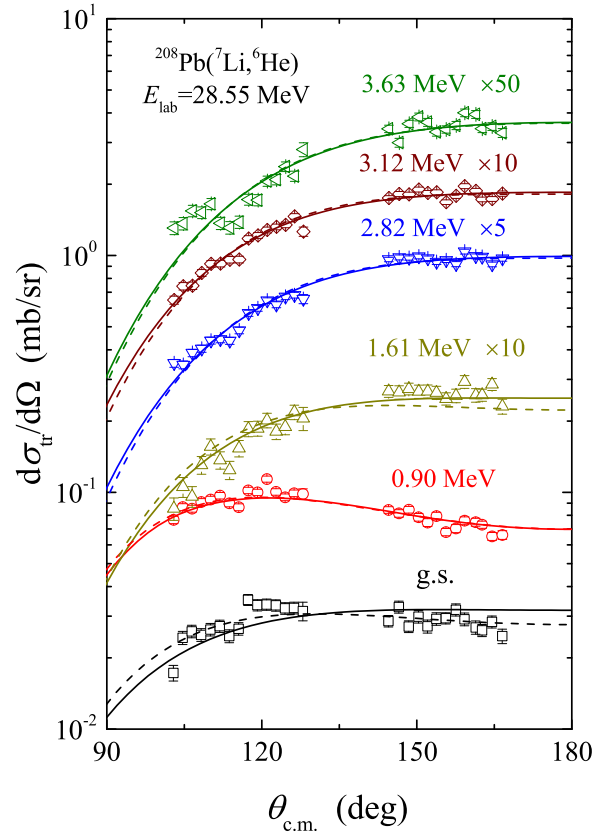

FIG. 5. Angular distributions of ^{208}Pb(^{7}Li,^{6}He) reactions for protons transferred to different states of ^{209}Bi at $E_{\rm lab}$ = 28.55 MeV. Experimental results are labeled according to the excitation energy of ^{209}Bi. Solid and dashed curves represent the CRC and DWBA fitting results, respectively.

the cross section of the transfer reaction will decrease rapidly as the energy decreases in the subbarrier region, as shown in Fig. 4, where the spectrum recorded by the last two layers of the telescope at $E_{\rm lab}$ = 24.30 MeV is presented. In this case, only the final states of protons transferred to the ground as well as the first excited states of ^{209}Bi can be identified. While for the lowest incident energy, $E_{\rm lab}$ = 21.20 MeV, only the ground state of ^{209}Bi was observed as the final state. Finally, the angular distributions of these transfer reactions are presented in Figs. 5 to 7, respectively. Only the statistical errors are taken into account for the transfer reaction data.

III. DATA ANALYSIS AND DISCUSSION

In this section, the transfer reaction method is introduced first, followed by a data analysis of the elastic scattering of the entrance channel, as well as the transfer reaction. The energy dependence of the OMP of the halo system ^{6}He + ^{209}Bi is discussed last. The standard Woods-Saxon shape is adopted for the optical potential, and all the calculations in the present work were performed by the code FRESCO [29]. Details of the expression form of the OMP, as well as the optical model (OM), distorted-wave Born approximation (DWBA), and coupled reaction channel (CRC) calculations, are described in Ref. [18].

A. Transfer reaction method

For a transfer reaction $a + A \rightarrow b + B$, assuming $a = b + x$ and $B = A + x$, where x denotes the transferred particle and moves from a to A. In the DWBA calculation, the transfer amplitude T can be expressed as

$$T = \int \chi_f^{(-)\star}(\vec{k}_f,\vec{r}_f) G(\vec{r}_i,\vec{r}_f) \chi_i^{(+)}(\vec{k}_i,\vec{r}_i) d\vec{r}_i d\vec{r}_f, \qquad (1)$$

where $\chi_i^{(+)}$ and $\chi_f^{(-)}$ are the ingoing and outgoing distorted waves, which describe the elastic scattering in the initial and final channels, respectively. The transfer function $G(\vec{r}_i,\vec{r}_f)$ can be given as

$$G(\vec{r}_i,\vec{r}_f) = \Psi_B^\star(\vec{r_{2x}}) V_{if} \Psi_a^\star(\vec{r_{1x}}), \qquad (2)$$

where Ψ_a and Ψ_B are the bound-state wave functions for the transferred particle x bound to the cores b and A, with $\vec{r_{1x}}$ and $\vec{r_{2x}}$ denoting the internal coordinates of the initial and final fragments, respectively. V_{if} represents the interaction between the initial and the final states.

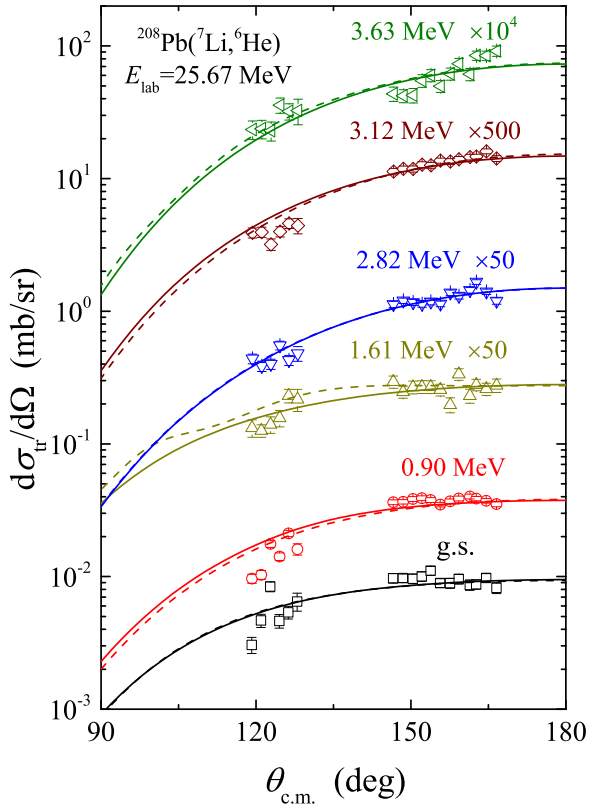

FIG. 6. Same as Fig. 5, but for the incident energy of E_{lab} = 25.67 MeV.

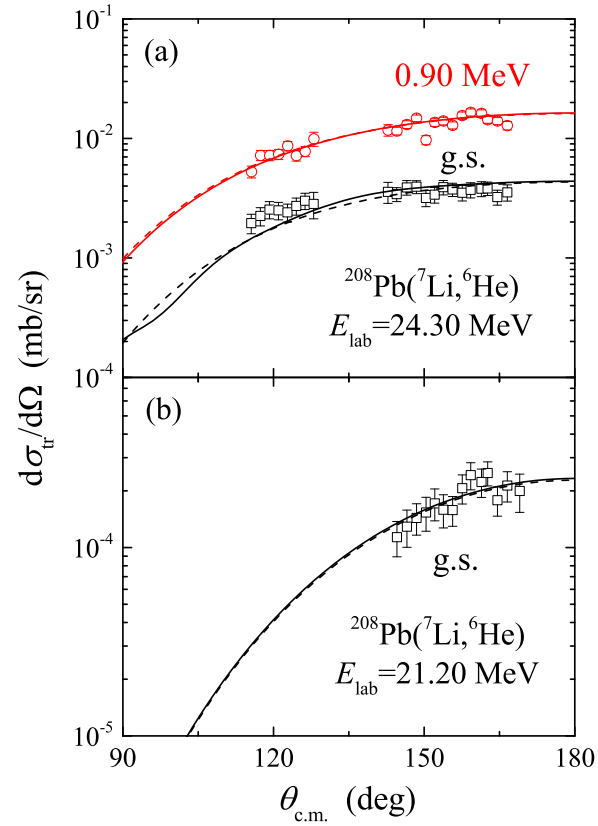

FIG. 7. Same as Fig. 5, but for the incident energies of (a) E_{lab} = 24.30 MeV and (b) E_{lab} = 21.20 MeV.

According to the above equations, four wave functions are needed in the DWBA calculation. The two bound-state wave functions can be calculated well by means of the single-particle potential model [30,31]. The wave functions of the two scattering states can be generated from appropriate optical potentials. For the ingoing channel, with the high-quality stable beam, measurement of the angular distribution of elastic scattering with a high precision is easy and the optical potential can be determined reliably. Thus, by fitting the angular distribution of the transfer reaction, the only unknown optical potential of the exit channel can be extracted [23].

The greatest advantage of this method is that, instead of low-intensity radioactive ion beams, a stable beam with a high intensity and quality can be employed to induce the transfer reaction, thus a more precise OMP of the exotic system can be expected. Moreover, the cross section of the transfer reaction can provide an additional constraint on the OMP to ensure the precision of the result. It is more significant in the subbarrier region, where the nuclear interaction becomes insensitive to the elastic scattering angular distribution, which turns out to be flat due to the strong Coulomb repulsive effect, leading to large uncertainties in the OMP parameters. For the transfer reaction, however, a distinct nuclear potential is required to overcome the Coulomb interaction and fulfill the reaction process, indicating that a stronger constraint on the nuclear potential can be provided by the transfer reaction data. It can be verified by the sensitivity test described in Ref. [24]. Here, this investigation is extended to a deep subbarrier energy, i.e., the lowest incident energy we measured [E_{lab}(^{7}Li) = 21.20 MeV], and compared with the calculated results for the elastic scattering of ^{6}He + ^{209}Bi at the corresponding energy [$E_{c.m.}$(^{6}He) = 14.34 MeV]. In the calculations, all other parameters are fixed, leaving V and W of ^{6}He + ^{209}Bi varied at a certain step. The calculated angular distributions of the transfer reaction and the elastic scattering are shown in Fig. 8. It can be seen that at the deep subbarrier energy, neither the angular distributions of the transfer reaction nor that of the elastic scattering are as sensitive to the optical potential as those in the above-barrier region [24], especially for the real part. Thus large uncertainties in the OMP parameters will be introduced due to this insensitivity. However, there are still differences in the results extracted from the transfer reaction versus the elastic scattering. To demonstrate this difference explicitly, we define the variable "sensitivity" s as

$$s = d\sigma/dV(W), \tag{3}$$

where $d\sigma$ is the relative variation of the differential cross section of the transfer reaction (in units of mb/sr) or that of the elastic scattering (described as the ratio to Rutherford), at the most backward angle, and $dV(W)$ is the corresponding relative variation of the real (imaginary) potential. For the transfer reaction, the s values for the real and imaginary parts are 0.021 and 0.093, while for the elastic scattering, the corresponding s values are 0.0017 and 0.033, respectively. This result indicates that with the condition of the same

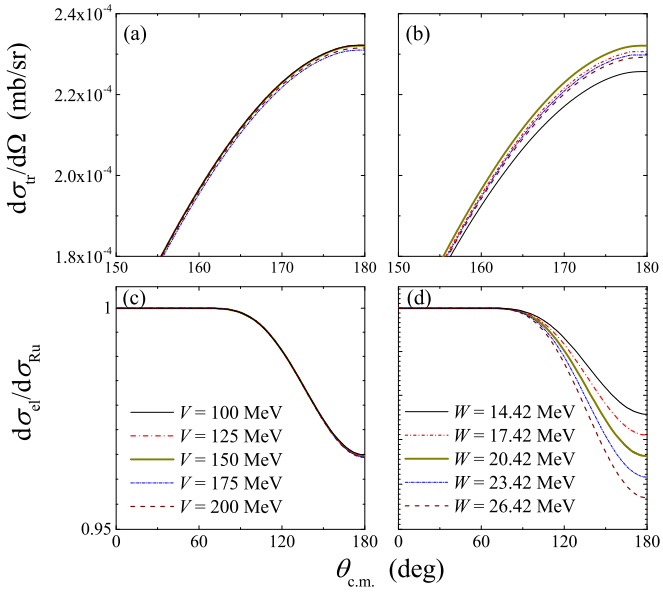

FIG. 8. Variations of angular distributions of ^{208}Pb(^{7}Li,^{6}He)^{209}Bi with (a) V and (b) W of ^{6}He + ^{209}Bi in the exit channel at $E_{lab}(^{7}\text{Li}) =$ 21.20 MeV. (c, d) Corresponding results for elastic scattering of ^{6}He + ^{209}Bi at the responsible energy $E_{c.m.}(^{6}\text{He}) = 14.34$ MeV.

statistical error, the uncertainties of the real and imaginary potentials extracted from the transfer reaction will be reduced by 12 and 3 times, compared with the regular elastic scattering measurement.

Furthermore, different final states of the transfer reaction can be obtained simultaneously, which is favorable for investigation of the energy dependence of the optical potential. With the population of higher excited states, the kinetic energy of the exit system will be pushed to a lower region, which is very helpful for extraction and study of the optical potential at energies well below the Coulomb barrier.

B. Elastic scattering of ^{7}Li + ^{208}Pb

The OMP parameters of the entrance channel ^{7}Li + ^{208}Pb are required as the input of the transfer reaction calculation. Therefore, the elastic scattering of ^{7}Li + ^{208}Pb is analyzed first, to extract the OMPs of this weakly bound system.

First, a grid search on all six parameters, $\{X_i\} = \{V, r_{0V}, a_V, W, r_{0W}, a_W\}$ (r_0 and a represent the reduced interaction radius and diffuseness parameter, respectively), was carried out with the OM, to obtain the best fit to the elastic scattering angular distributions at different bombarding energies. The "goodness-of-fit" quantity is described by χ^2 analysis. The extracted parameters are then used as the initial values in CRC calculations. The details of the CRC coupling scheme are demonstrated in Ref. [18]. The fitting results of the OM as well as the CRC approach are presented in Fig. 3, by the dashed and solid curves, respectively. It can be seen that the potential parameters obtained by both the OM and the CRC methods describe the experimental data satisfactorily. The extracted potential parameters are listed in Table I. It is noteworthy that the goal of the entrance channel analysis is just to extract the appropriate OMP parameters as the input of the transfer reaction calculations, rather than to discuss the global tendency of the OMP of the ^{7}Li + ^{208}Pb system. Thus only the best fitting results are listed [18,27].

TABLE I. OMP parameters of ^{7}Li + ^{208}Pb extracted from the elastic scattering by the OM and CRC fittings.

	E_{lab} (MeV)	V (MeV)	r_{0V} (fm)	a_V (fm)	W (MeV)	r_{0W} (fm)	a_W (fm)	χ^2/pt
OM	21.20	1.01	1.27	0.40	6.04×10^{-8}	1.25	0.64	0.20
	24.30	1.05	1.07	0.55	6.17×10^{-12}	1.25	0.62	0.63
	25.67	8.02	1.33	0.58	3.45×10^{-4}	1.22	0.52	0.11
	28.55	13.33	1.10	0.62	2.38	1.50	0.68	0.24
CRC	21.20	1.61	0.93	0.43	6.36×10^{-8}	1.40	0.59	0.36
	24.30	29.67	1.20	0.57	2.56×10^{-4}	1.19	0.61	0.68
	25.67	16.69	1.25	0.54	1.60×10^{-5}	0.75	0.42	0.16
	28.55	8.54	1.32	0.41	0.56	1.67	0.60	0.10

C. Transfer reactions of ^{208}Pb(^{7}Li,^{6}He)^{209}Bi

With the OMPs of the ^{7}Li + ^{208}Pb to describe the interaction of the entrance channel, the angular distributions of one-proton transfer reactions ^{208}Pb(^{7}Li,^{6}He)^{209}Bi could be analyzed further with the DWBA and CRC approaches, respectively, to extract the OMP of the halo nuclear system ^{6}He + ^{209}Bi in the exit channel. The energies of the whole data set discussed in this paper are listed in Table II. The details of the fitting procedure are presented below.

1. General description

Postrepresentation is adopted for both the DWBA and the CRC approaches, with the full complex remnant term considered. And the "core-core" interaction potential is taken from Ref. [32], where the global optical potential of ^{6}He at low energies is discussed. In the CRC calculation, ^{7}Li + ^{208}Pb inelastic scattering for the transitions to the first three excited states of ^{7}Li, as well as the reorientations of these states, is included in the coupling scheme. Excitations of ^{7}Li are described within a collective model. In addition, coupling effects of one-proton and one-neutron transfers are also considered [18].

2. Geometry parameters of the OMP of the exit channel

The geometry parameters of the OMP of the exit channel ^{6}He + ^{209}Bi are fixed as $r_{0V} = 1.02$ fm, $a_V = 0.70$ fm, $r_{0W} =$ 1.25 fm, and $a_W = 0.95$ fm [18], leaving the potential depths V and W to be searched.

3. Description of the interaction of bound states

According to the sensitivity test [24], the calculation results depend strongly on the radius parameter r_0 of the bound-state potential, i.e., a slight variation of r_0 will induce a large change in the amplitude of the differential cross section. Thus to describe the interaction of the bound state correctly, an accurate value of r_0, rather than the so-called "standard" value of 1.25 fm, should be employed. One effective method for deducing

TABLE II. Energies of the data set discussed in this paper.

$E_{lab}(^7Li)$	$E^*(^{209}Bi)$[a]	$E_{c.m.}(^6He)$[b]
21.20	0.00	14.34
24.30	0.00	17.34
	0.90	16.45
25.67	0.00	18.66
	0.90	17.77
	1.61	17.05
	2.82	15.84
	3.12	15.54
	3.63	15.03
28.55	0.00	21.45
	0.90	20.56
	1.61	19.84
	2.82	18.63
	3.12	18.33
	3.63	17.82
32.55[c]	0.00	25.31
	0.90	24.41
	1.61	23.70
37.55[c]	0.00	30.14
	0.90	29.25
	1.61	28.54
42.55[c]	0.00	34.99
	0.90	34.09
	1.61	33.37

[a]The excitation energy of ^{209}Bi as the final state of ^{208}Pb(^{7}Li,^{6}He)^{209}Bi.
[b]The corresponding reaction energy of ^{6}He + ^{209}Bi in the center-of-mass frame.
[c]Taken from previous work [18].

the rms radius (r_{rms}) of the valence proton is the knockout reaction with a high-energy electron (e,$e'p$). Therefore, r_0 can be extracted accurately by reproducing r_{rms} obtained from the corresponding (e,$e'p$) experimental data. According to the results in Refs. [33] and [34], the r_0's of ^{7}Li and ^{209}Bi are determined to be 1.87 and 1.21 fm, respectively, which are adopted in the present calculations.

4. *Spectroscopic factors*

For ^{7}Li, the spectroscopic factor (S factor) of protons in the ground state is fixed at 0.60, which is taken from Ref. [35]. As the excited states of ^{7}Li are described with the collective model in CRC calculations, only the S factor of the ground state is taken into account. For ^{209}Bi, however, with the values taken from Ref. [36] as initial inputs, the S factors of different single-particle states, as well as the OMP parameters, are extracted simultaneously by fitting the experimental data. The extracted S factors are listed in Table III.

Finally, the fitting results with the CRC and DWBA approaches are shown in Figs. 5–7, by the solid and dashed curves, respectively. The extracted V and W at the sensitive radius 13.5 fm [18] are presented in Figs. 9(a) and 9(b), where filled circles and open squares represent the CRC and DWBA results, respectively. The errors are derived by χ^2 analysis as described in Ref. [37], with a confidence level of 68.3%. In

TABLE III. Extracted S factors for ^{209}Bi.

E^* (MeV)[a]	Configuration	S factor
0.0	$1h_{9/2}$	1.16±0.04[b]
0.90	$2f_{7/2}$	0.87±0.05[b]
1.61	$1i_{13/2}$	0.49±0.11[b]
2.82	$2f_{5/2}$	0.75±0.04
3.12	$3p_{3/2}$	0.77±0.06
3.63	$3p_{1/2}$	0.36±0.05

[a]Excitation energy.
[b]Taken from Ref. [18].

Fig. 9, results taken from the previous work [18] at energies of 32.55, 37.55, and 42.55 MeV are also shown, by the stars.

The reliability of the extracted OMP parameters is confirmed by calculating the elastic scattering of ^{6}He + ^{209}Bi and comparing it with the experimental elastic scattering data at the corresponding energies, as shown in Fig. 10. It can be seen

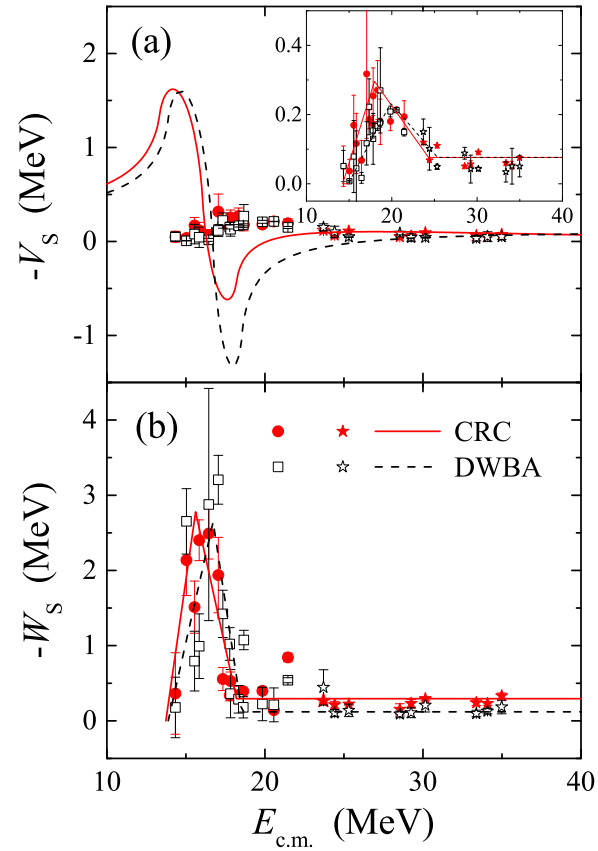

FIG. 9. Energy dependence of the (a) real and (b) imaginary potentials at the sensitivity radius of 13.5 fm for the ^{6}He + ^{209}Bi system. Filled circles and open squares represent CRC and DWBA results from the present work; filled and open stars denote CRC and DWBA results taken from Ref. [18]. Solid and dashed curves in (b) represent the linear segment fitting for the imaginary potential derived by the CRC and DWBA approaches. The predictions of the dispersion relation according to the variations of the imaginary potentials are presented in (a) by the corresponding curves for the CRC and DWBA results. Inset in (a): Fine structure of the real potential.

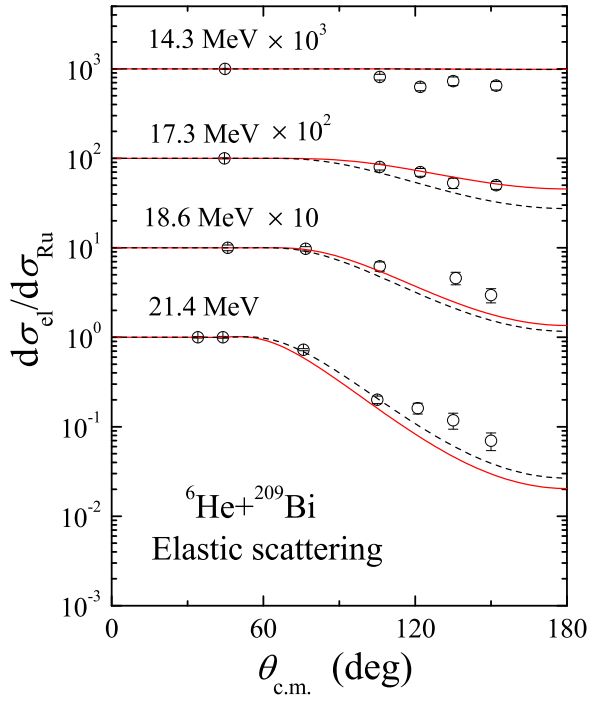

FIG. 10. Elastic scattering angular distributions of the ^{6}He + ^{209}Bi system. Open circles represent experimental data taken from Refs. [38] and [39]. Solid and dashed curves are calculation results with OMP parameters extracted through the CRC and DWBA methods, respectively.

that the OMPs extracted by both the CRC and the DWBA methods reproduce the elastic scattering data properly, except at the lowest energy, where the calculated results overestimate the experimental data. This may arise from the uncertainty in the normalization of the experimental data owing to the intrinsic difficulty at such a low energy [14].

Moreover, the similarities between the calculation results with CRC and those with DWBA parameters indicate that for the transfer reaction ^{208}Pb(^{7}Li,^{6}He)^{209}Bi, there are no strong coupling effects from the entrance channel. Since the main difference between the CRC and the DWBA approaches is that a relatively pure effective potential of the exit channel is expected in the CRC calculations by considering the couplings arising from the entrance channel explicitly and excluding the influence of the entrance channel to a certain extent, while in the DWBA calculations, such influences originating from the couplings between ^{7}Li and ^{6}He cannot be removed from the OMPs of the exit channel. This difference is very significant when the transfer method is applied to the reaction ^{63}Cu(^{7}Li,^{6}He) to study the OMP of the halo nuclear system ^{6}He + ^{64}Zn [27], for which only the CRC parameters can reproduce the experimental elastic scattering data. However, the calculation results with CRC and DWBA parameters in the present work are almost the same, indicating that compared with the odd-A and medium-mass nuclear system ^{7}Li + ^{63}Cu, the coupling effects of ^{7}Li interacting with the heavy target ^{208}Pb are much weaker.

D. Energy dependence of the OMP of ^{6}He + ^{209}Bi

As shown in Fig. 9, strong energy dependence is observed for both the real and the imaginary parts. According to the linear-segment fitting as shown in the inset in Figs. 9(a) and 9(b), the CRC and DWBA results are expressed as

$$V = \begin{cases} 0.080E_{\mathrm{c.m.}} - 1.13, & E_{\mathrm{c.m.}} \leqslant 17.97, \\ -0.032E_{\mathrm{c.m.}} + 0.86, & 17.97 < E_{\mathrm{c.m.}} \leqslant 24.30, \\ 0.076, & E_{\mathrm{c.m.}} > 24.30, \end{cases} \tag{4a}$$

$$W = \begin{cases} 0, & E_{\mathrm{c.m.}} \leqslant 13.73, \\ 1.48E_{\mathrm{c.m.}} - 20.26, & 13.73 < E_{\mathrm{c.m.}} \leqslant 15.62, \\ -0.96E_{\mathrm{c.m.}} + 17.77, & 15.62 < E_{\mathrm{c.m.}} \leqslant 18.20, \\ 0.29, & E_{\mathrm{c.m.}} > 18.20, \end{cases} \tag{4b}$$

and

$$V = \begin{cases} 0.047E_{\mathrm{c.m.}} - 0.70, & E_{\mathrm{c.m.}} \leqslant 19.89, \\ -0.034E_{\mathrm{c.m.}} + 0.91, & 19.89 < E_{\mathrm{c.m.}} \leqslant 25.36, \\ 0.076, & E_{\mathrm{c.m.}} > 25.36, \end{cases} \tag{5a}$$

$$W = \begin{cases} 0, & E_{\mathrm{c.m.}} \leqslant 13.88, \\ 0.93E_{\mathrm{c.m.}} - 12.92, & 13.88 < E_{\mathrm{c.m.}} \leqslant 16.72, \\ -1.39E_{\mathrm{c.m.}} + 25.87, & 16.72 < E_{\mathrm{c.m.}} \leqslant 18.54, \\ 0.12, & E_{\mathrm{c.m.}} > 18.54, \end{cases} \tag{5b}$$

respectively, where the energy is given in units of MeV. It should be kept in mind that these functions are derived from the potential depths at the sensitive radius (13.5 fm), rather than the center depths.

The extracted OMPs are effective potentials. As the bare potential is nearly energy independent, this strong energy dependence mainly arises from the dynamic polarization potential (DPP), which includes all coupling effects to nonelastic direct reaction channels.

For the real part of the OMP, a maximum is present around the Coulomb barrier ($V_B \approx 20$ MeV in the center-of-mass system), demonstrating an attractive polarization effect. Such an attractive DPP may further reduce the fusion barrier, resulting in an increase in the fusion probability in the subbarrier energy region. This has been confirmed by the previous experimental data [40], where a large fusion enhancement at subbarrier energies was observed. On the other hand, an important feature of weakly bound nuclear systems is their collective response, such as soft dipole resonance, which has been confirmed in ^{6}He [41] and may play an important role, especially in the subbarrier region. Together with the extended matter distribution, the soft dipole resonance, rather than the breakup, will lead to the observed enhancement of the fusion cross section, as well as the observed attractive DPP [42].

The energy dependence of the imaginary potential attracts great attention nowadays, especially that of the weakly bound nuclear system, which exhibits abnormal behaviors, such as an increasing trend of the imaginary potential as the interaction energy decreases in the subbarrier region. Although great

efforts have been devoted, there are still several long-standing questions about the imaginary potential, such as whether the increasing trend will be continued and whether there exists a turning point, after which the imaginary potential begins to decrease and then the threshold energy emerges. To address these questions, the potential at sufficiently low energies is required. With the help of the transfer reaction method, we get the opportunity to shed some light on this region.

As shown in Fig. 9(b), the depth increases first as the interaction energy decreases in the subbarrier region, demonstrating that some reaction channels are still open even though there exists a strong Coulomb repulsive effect. It naturally connects with the breakup process due to the low separation energy of the weakly bound system. However, the experimental results for ^{6}He + ^{209}Bi [43,44] show that the predominant reactions in the subbarrier region are one- and two-neutron transfer, rather than the breakup process. Moreover, as the energy drops further, a decreasing trend is clearly observed, which vanishes at 13.73 ± 1.63 MeV (with a confidence interval of 90%) according to the extrapolation. Thus the threshold can be determined as $0.68V_B$. This is the first time that in a halo nuclear system the decrease in the imaginary potential is observed in a deep subbarrier region, and the threshold emerges. This threshold indicates that all nonelastic channels are effectively closed by the Coulomb barrier, and reactions occur only when the interaction energy rises above this threshold energy to overcome the repulsive Coulomb interaction. To demonstrate the threshold explicitly, the distance of closest approach in the Coulomb field for a head-on collision at this energy is calculated, which is about $17.41^{+2.35}_{-1.85}$ fm. This result is in good agreement with the critical interaction distance (18.91 ± 1.24 fm) extracted from the elastic backscattering data [45]. So far, the threshold is only observed in some tightly bound systems and a few weakly bound systems. For example, for the tightly bound system ^{16}O + ^{208}Pb, the threshold energy can be determined easily as about $0.93V_B$ [3]. For the stable weakly bound nucleus ^{6}Li, on the other hand, the decreasing trend of the imaginary potential was observed only in a few medium-mass target systems, such as ^{6}Li + ^{80}Se [20] and ^{6}Li + ^{144}Sm [21], with a threshold energy of about $0.76V_B$ and $0.81V_B$, respectively. However, for a heavy target system as investigated in the present work, no similar result has been reported so far, because the imaginary potential still presents an increasing trend at the lowest energies, such as $0.86V_B$ for ^{6}Li + ^{208}Pb [46] and $0.94V_B$ for ^{9}Be + ^{209}Bi [47]. The low threshold energy further demonstrates the low binding energy and extended matter distribution of the halo nucleus ^{6}He.

E. Applicability of the dispersion relation

Considering the energy dependence, the OMP can be expressed as

$$U(r;E) = V(r;E) + iW(r;E), \tag{6}$$

where

$$V(r;E) = V_0(r;E) + \Delta V(r;E). \tag{7}$$

$V_0(r;E)$ is slowly and smoothly energy dependent, which arises from the nonlocality effects, and $\Delta V(r;E)$ is the DPP resulting from the time nonlocality and can be linked to the imaginary potential $W(r;E)$ with the dispersion relation

$$\Delta V(r;E) = \frac{P}{\pi}\int \frac{W(r;E')}{E'-E}dE', \tag{8}$$

where P denotes the principal value of the integral.

The dispersion relation is derived from the Kramers-Kronig relations, which is based on the causality principle and used to describe the effect of dispersion in a medium on the properties of a wave traveling within that medium. The Kramers-Kronigs relations [48], in a more general case, are mathematical relations, connecting the real and imaginary parts of any complex function of stable systems that is analytic in the upper half-plane. This relation is derived from Cauchy's residue theorem, which demands that there should be a finite list of isolated singularities in the real axis. In the case of nuclear physics, these isolated singularities correspond to the discrete bound states of the interacting system.

The effectiveness of the dispersion relation in tightly bound nuclear systems has been confirmed by many experimental data [4]. However, its applicability in the weakly bound nuclear system is still debatable. For example, in the case of ^{6,7}Li + ^{28}Si [49,50], the dispersion relation cannot describe the connection between the real and the imaginary potentials properly. For the halo systems ^{6}He + ^{209}Bi [14] and ^{8}B + ^{58}Ni [51], it seems to work well within the uncertainties. However, due to the lack of complete information on the imaginary potential in the deep subbarrier region, a convincing conclusion cannot be drawn. As shown in Ref. [14], the dispersion relation calculations varied significantly when a different threshold and turning point in imaginary potential were assumed. With the precise optical potential extracted in the present work, we get the opportunity to reexamine the applicability of the dispersion relation in ^{6}He + ^{209}Bi.

According to the linear segment fitting results of the imaginary potential as shown in Fig. 9(b), the dispersion relation calculation results with the linear schematic model [4] for the real part are shown in Fig. 9(a). It can be seen that the calculation results demonstrate a repulsive DPP in the subbarrier region, followed by an attractive one as the energy decreases further. Obviously, this prediction is inconsistent with the experimental results, indicating that the dispersion relation does not hold for the halo system ^{6}He + ^{209}Bi. This result is surprising but interesting. Since the dispersion relation arises from the causality principle, it is a natural idea that this relation should be universal for every system. We list possible reasons for the failure of the dispersion relation, which may be only some hints to understanding this abnormal behavior, and the underlying physics strongly calls for further research.

The OMP extracted from experimental data is a phenomenological potential, rather than the generalized optical potential [52], which is nonlocal, and yields the unaveraged elastic scattering amplitude. However, the phenomenological OMP is local and can be employed directly to solve the Schrödinger equation for the scattering amplitude averaged over a suitable energy interval. An additional energy depen-

dence, which can be called the *spurious energy dependence* [53], is introduced in the equivalent local potential. The spurious energy dependence does not follow the dispersion relation and could be more significant when the nonlocality is of the order of magnitude of the incident wavelength [52]. It is assumed that the long-range effects of nonlocality can be represented by a smooth and slow variation with energy and seem to have little effect on the rapid variation of the potential around the Coulomb barrier. However, according to the results of recent research, the nonlocal potential is important to describe reactions induced by deuterons and to correct the energy dependence of the potential [54,55]. These results indicate the importance of nonlocality effects, which should be considered in discussion of the dispersion relation when concerned with the weakly bound system.

On the other hand, the optical potential extracted from the experiment is only reliable within a certain region where the OMP parameters can be determined accurately. The location of the sensitive region is crucial information before we can discuss the OMP meaningfully. There are several methods to extract the sensitive region, such as the crossing-point method [56] and notch technique [57]. It is well known that both the elastic scattering and the transfer reaction are peripheral processes, thus the extracted OMPs are only sensitive to the region located in the external part of the potential. Even though a beam with an extremely high energy is used, e.g., for the system $p + {}^{12}\mathrm{C}$ with an incident proton energy of 1.04 GeV, only the external part of the potential can be probed, and the deep interior region of the nuclear potential is still invisible due to the effect of strong absorption [58]. As pointed out in Ref. [53], it remains an open question whether the phenomenological potentials also yield the correct off-energy-shell scattering amplitudes (i.e., the wave functions in the interior region). However, the dispersion relation is derived only for a potential that can yield the wave function over all spatial regions. Thus the phenomenological potential, which can only generate the wave function in the external region, does not necessarily need to abide by the causality property [53].

IV. SUMMARY AND CONCLUSIONS

In the present work, the angular distributions of transfer reactions $^{208}\mathrm{Pb}(^{7}\mathrm{Li},^{6}\mathrm{He})^{209}\mathrm{Bi}$ at deep subbarrier energies are measured. By fitting the experimental data with the CRC and DWBA methods, the OMP parameters of the halo system $^{6}\mathrm{He} + {}^{209}\mathrm{Bi}$ are extracted precisely. The results of the CRC and DWBA methods are very similar to each other, indicating that for the heavy interaction system, there is no strong coupling effect between the entrance and the exit channels. Combined with results of the previous work [18], a strong energy dependence is observed in both the real and the imaginary potentials. For the real part, a bell-like shape is present around the Coulomb barrier, which is similar to the behavior of the tightly bound nuclear system. For the imaginary potential, however, an abnormal behavior is clearly observed: as the energy decreases in the subbarrier region, the imaginary potential first increases, then decreases with a further reduction in the energy, and the threshold emerges. This is the first time that the threshold can be determined clearly for a halo nuclear system. Moreover, the classical dispersion relation cannot be adopted to describe the connection between the real and the imaginary parts, and several possible reasons are discussed; the underlying physics strongly deserves further research.

With the great advantages of the transfer reaction method, a complete picture of the OMP of the halo system $^{6}\mathrm{He} + {}^{209}\mathrm{Bi}$ is obtained for the first time, and all of the distinctive features of the OMPs are mainly from the couplings to the continuum states of $^{6}\mathrm{He}$ due to its halo structure, which can help us to obtain a more complete and intensive understanding of the properties of the OMPs of weakly bound systems.

ACKNOWLEDGMENTS

This work was supported by the National Key Basic Research Program of China (Grant No. 2013CB834404) and by the National Natural Science Foundation of China (Grants No. 11505293, No. 11635015, No. 11375268, No. 11475263, No. U1432246, and No. U1432127).

[1] N. Keeley, N. Alamanos, K. W. Kemper, and K. Rusek, Prog. Part. Nucl. Phys. **63**, 396 (2009).
[2] B. R. Fulton, D. W. Banes, J. S. Lilley *et al.*, Phys. Lett. B **162**, 55 (1985).
[3] M. A. Nagarajan, C. C. Mahaux, and G. R. Satchler, Phys. Rev. Lett. **54**, 1136 (1985).
[4] C. Mahaux, H. Ngô, and G. R. Satchler, Nucl. Phys. A **449**, 354 (1986).
[5] L. F. Canto, P. R. S. Gomes, R. Donangelo *et al.*, Phys. Rep. **596**, 1 (2015).
[6] Y. Kucuk, I. Boztosun, and N. Keeley, Phys. Rev. C **79**, 067601 (2009).
[7] A. Di Pietro, G. Randisi, V. Scuderi *et al.*, Phys. Rev. Lett. **105**, 022701 (2010).
[8] R. S. Mackintosh and N. Keeley, Phys. Rev. C **70**, 024604 (2004).
[9] N. Keeley and R. S. Mackintosh, Phys. Rev. C **71**, 057601 (2005).
[10] K. Rusek, N. Keeley, K. W. Kemper, and R. Raabe, Phys. Rev. C **67**, 041604(R) (2003).
[11] A. M. Sánchez-Benítez, D. Escrig, M. A. G. Álvarez *et al.*, Nucl. Phys. A **803**, 30 (2008).
[12] A. Bonaccorso and F. Carstoiu, Nucl. Phys. A **706**, 322 (2002).
[13] A. A. Ibraheem and A. Bonaccorso, Nucl. Phys. A **748**, 414 (2005).
[14] A. R. Garcia, J. Lubian, I. Padron, P. R. S. Gomes, T. Lacerda, V. N. Garcia, A. Gómez Camacho, and E. F. Aguilera, Phys. Rev. C **76**, 067603 (2007).
[15] N. Keeley, S. J. Bennett, N. M. Clarke *et al.*, Nucl. Phys. A **571**, 326 (1994).
[16] C. Signorini, A. Andrighetto, M. Ruan *et al.*, Phys. Rev. C **61**, 061603(R) (2000).
[17] M. S. Hussein, P. R. S. Gomes, J. Lubian, and L. C. Chamon, Phys. Rev. C **73**, 044610 (2006).
[18] L. Yang, C. J. Lin, H. M. Jia *et al.*, Phys. Rev. C **89**, 044615 (2014).

[19] A. Gómez Camacho, E. F. Aguilera, E. Martínez Quiroz *et al.*, Nucl. Phys. A **833**, 156 (2010).
[20] L. Fimiani, J. M. Figueira, G. V. Martí *et al.*, Phys. Rev. C **86**, 044607 (2012).
[21] J. M. Figueira, J. O. Fernández Niello, A. Arazi *et al.*, Phys. Rev. C **81**, 024613 (2010).
[22] M. A. Tiede, D. E. Trcka, and K. W. Kemper, Phys. Rev. C **44**, 1698 (1991).
[23] C. J. Lin, F. Yang, P. Zhou *et al.*, AIP Conf. Proc. **853**, 81 (2006).
[24] Z. D. Wu, L. Yang, C. J. Lin *et al.*, Chin. Phys. Lett. **31**, 092401 (2014).
[25] G. P. An, C. J. Lin, H. Q. Zhang *et al.*, Chin. Phys. Lett. **25**, 4237 (2008).
[26] Z. D. Wu, C. J. Lin, H. Q. Zhang *et al.*, Chin. Phys. Lett. **26**, 022503 (2009).
[27] L. Yang, C. J. Lin, H. M. Jia *et al.*, Phys. Rev. C **95**, 034616 (2017).
[28] L. Yang, C. J. Lin, H. M. Jia *et al.*, Phys. Rev. Lett. **119**, 042503 (2017).
[29] I. J. Thompson, Comp. Phys. Rep. **7**, 167 (1988).
[30] C. J. Lin, H. Q. Zhang, Z. H. Liu, Y. W. Wu, F. Yang, and M. Ruan, Phys. Rev. C **66**, 067302 (2002).
[31] R. Sherr, Phys. Rev. C **54**, 1177 (1996).
[32] Y. Kucuk, I. Boztosun, and T. Topel, Phys. Rev. C **80**, 054602 (2009).
[33] L. Lapikás, J. Wesseling, and R. B. Wiringa, Phys. Rev. Lett. **82**, 4404 (1999).
[34] D. Branford, A. W. Rauf, J. Lác *et al.*, Phys. Rev. C **63**, 014310 (2000).
[35] A. M. Moro, J. Gómez-Camacho, I. Martel *et al.*, Nucl. Phys. A **628**, 203 (1998).
[36] C. Ellegaard, P. Vedelsby, Phys. Lett. B **26**, 155 (1968).
[37] D. Abriola, A. Arazi, J. Testoni *et al.*, J. Phys.: Conf. Ser. **630**, 012021 (2015).
[38] E. F. Aguilera, J. J. Kolata, F. M. Nunes *et al.*, Phys. Rev. Lett. **84**, 5058 (2000).
[39] E. F. Aguilera, J. J. Kolata, F. D. Becchetti *et al.*, Phys. Rev. C **63**, 061603(R) (2001).
[40] J. J. Kolata, V. Guimarães, D. Peterson *et al.*, Phys. Rev. Lett. **81**, 4580 (1998).
[41] S. Nakayama, T. Yamagata, H. Akimune *et al.*, Phys. Rev. Lett. **85**, 262 (2000).
[42] M. S. Hussein, L. F. Canto, and R. Donangelo, Nucl. Phys. A **722**, C321 (2003).
[43] P. A. DeYoung, P. J. Mears, J. J. Kolata *et al.*, Phys. Rev. C **71**, 051601(R) (2005).
[44] J. P. Bychowski, P. A. DeYoung, B. B. Hilldore *et al.*, Phys. Lett. B **596**, 26 (2004).
[45] V. Guimarães, J. J. Kolata, E. F. Aguilera *et al.*, Phys. Rev. C **93**, 064607 (2016).
[46] C. L. Zhang, H. Q. Zhang, C. J. Lin *et al.*, Chin. Phys. Lett. **23**, 1146 (2006).
[47] N. Yu, H. Q. Zhang, H. M. Jia *et al.*, J. Phys. G: Nucl. Part. Phys. **37**, 075108 (2010).
[48] Taken from Wikipedia, https://en.wikipedia.org/wiki/Kramers-Kronig_relations.
[49] A. Pakou, N. Alamanos, A. Lagoyannis *et al.*, Phys. Lett. B **556**, 21 (2003).
[50] A. Pakou, N. Alamanos, G. Doukelis *et al.*, Phys. Rev. C **69**, 054602 (2004).
[51] A. Gómez Camacho, E. F. Aguilera, P. R. S. Gomes, and J. Lubian, Phys. Rev. C **84**, 034615 (2011).
[52] G. Passatore, Nucl. Phys. A **95**, 694 (1967).
[53] R. Lipperheide and A. K. Schmidt, Nucl. Phys. A **112**, 65 (1968).
[54] N. K. Timofeyuk and R. C. Johnson, Phys. Rev. C **87**, 064610 (2013).
[55] N. K. Timofeyuk and R. C. Johnson, Phys. Rev. Lett. **110**, 112501 (2013).
[56] C. J. Lin, J. C. Xu, H. Q. Zhang, Z. H. Liu, F. Yang, and L. X. Lu, Phys. Rev. C **63**, 064606 (2001).
[57] L. Yang, C. J. Lin, H. M. Jia *et al.*, Chin. Phys. C **40**, 056201 (2016).
[58] J. G. Cramer and R. M. DeVries, Phys. Rev. C **22**, 91 (1980).